National Conference with International Participation
ENGINEERING MECHANICS 2008
Svratka, Czech Republic, May 12 – 15, 2008

ANALYSIS OF COUPLED HEAT AND MOISTURE TRANSFER IN MASONRY STRUCTURES

J. Sýkora* **and J. Vorel***

Summary: *Evaluation of effective or macroscopic coefficients of thermal conductivity under coupled heat and moisture transfer is presented. The paper first gives a detailed summary on the solution of a simple steady state heat conduction problem with an emphasis on various types of boundary conditions applied to the representative volume element – a periodic unit cell. Since the results essentially suggest no superiority of any type of boundary conditions, the paper proceeds with the coupled nonlinear heat and moisture problem subjecting the unit cell to the prescribed macroscopically uniform heat flux. This allows for a direct use of the academic or commercially available codes. Here, the presented results are derived with the help of SIFEL and DELPHIN systems. A comment on treating internal interfaces, when materials with substantially different porosities are expected, is also provided.*

1 Introduction

An extensive experimental and numerical analysis of Charles Bridge in Prague has been performed only recently to identify the most severe external actions on the bridge, see e.g. (Novák et al., 2007; Sýkora et al., 2005; Šejnoha et al., 2005). Among others the loading due to spatially and temporarily varying temperature and moisture changes appeared to be of paramount importance as these effects proved as crucial factors responsible for the nucleation and further development of cracks in the bridge.

When dealing with these problems, the application of homogenization techniques is inevitable (Oezdemir et al., 2006). Solving a set of problem equations on a meso-scale (a composition of stone blocks and mortar) provides us with up-scaled macroscopic equations. They include a number of effective (macroscopic) transport parameters, which are necessary for a detailed analysis of the state of a structure as a whole. A reliable methodology of the prediction of these quantities is one of the main goals of our contribution. Any (multi-scale) approach to coupled heat and moisture transfer draws on a cogent description of transport phenomena.

*Ing. Jan Sýkora and Ing. Jan Vorel, Department of Mechanics, Faculty of Civil Engineering, Czech Technical University in Prague, Thkurova 7, 166 29 Prague 6, tel: (+420)-2-2435-4606, fax: (+420)-2-2431-077, e-mail: jan.sykora.1@fsv.cvut.cz, jan.vorel@fsv.cvut.cz

An extensive review of this topic can be found in (Černý and Rovnaníková, 2002). Averaging theories (a micromechanics-based approach), primarily formulated in (Hassanizadech and Gray, 1979a,b), can be regarded as a counterpart to phenomenological ones (a macromechanics-based approach), see (De Boer, 1996; Biot, 1941). Both approaches are explained in detail in (Lewis and Schrefler, 1999). The model described in this monograph is likely the most advanced hydro-thermo-mechanical approach so far employed for FE-based computations with account for the variation of porosity. Contrary to these trends, phenomenological models are still preferred to averaging ones, namely calculating the heat and moisture transfer in building materials.

As outlined in (Černý and Rovnaníková, 2002), the models for the description of water and water vapor transfer can broadly be classified into three main categories, namely convection models, diffusion models and hybrid models. The recognized convection model is that of Philip and de Vries, see e.g. (Philip and de Vries, 1957). A variety of diffusion models were developed based on Krischer's original version (Krischer, 1963). A certain drawback of this category lies in the absence of cross-effects between the heat and moisture transport. Krischer's model was improved by many authors. Let us at least introduce Künzel and Kiessl's model (Künzel and Kiessl, 1997). Despite the fact that the cross-effects are missing in this model it describes all substantial phenomena and its results comply well with experimentally obtained data. Because of the lack of space it is impossible to comment on further approaches such as hybrid models or complex models that require the application of irreversible thermomechanics, (Černý and Rovnaníková, 2002).

While models for transport processes have been developed during several decades, the computational methods for multi-scale modeling of these processes in masonry on meso and macro scales have emerged only recently. Moreover, most of them are prevailingly confined to the effective macroscopic description for heat conduction and employ the perturbation method to describe the fluctuations of temperature throughout the heterogeneous material. Different situations are analyzed using the homogenization method, which lead to different macroscopic descriptions in (Auriault, 1983). Boutin's model analyzing the microstructural influence on heat conduction belongs to the same category (Boutin, 1995). It is shown that the higher order terms introduce successive gradients of temperature and tensor characteristics of the microstructure, which result in non-local effects. An original approach to homogenization of transient heat transfer for some composite materials is proposed in (Kaminski, 2003). In that paper, the stochastic second moment perturbation method is used in conjunction with the finite element method. Probably the most complex multi-scale analysis for pure heat transfer in heterogeneous solids is offered in (Oezdemir et al., 2006). The authors established a macro to micro transition in terms of the applied boundary conditions and likewise a micro to macro transition formulated in the form of consistent averaging relations. See also (Tomková et al., 2007) for a similar study with applications to textile composites.

Homogenization strategies for coupled heat and mass transfer are rather an exception, see e.g. (Kaminski, 2003), and more or less belong to the modeling of a micro to meso rather than a meso to macro transition and vice versa. In this paper, the condition for a non-homogenizable situation, i.e. when it is impossible to find a macroscopic equivalent description, is also addressed. To our knowledge, the effective material parameters for fully coupled transfer processes in historical masonry structures (meso-macro approach) have been discussed so far only in (Sýkora et al., 2005).

The present paper is organized as follows. In Section 2, following the introductory part, we first review the basic formulas related to homogenization. These are subsequently used in Section 3 to estimate the effective thermal conductivities by solving a simple steady state heat

conduction problem. The main objective of this section is to address the effect of boundary conditions on the resulting homogenized properties. The fact that these properties are essentially invariant with respect to the choice of particular boundary conditions opens the way to the solution of the coupled heat and moisture transient problem. The essentials of theoretical formulation as well as some numerical results are presented in Section 4 clearly illustrating the effect of moisture on thermal conductivity and their dependence on varying material parameters, such as relative humidity and initial temperature. Section 5 then extends the theoretical background when internal interfaces are to be considered. Finally, the essential findings are summarized in Section 6.

2 Fundamentals of homogenization

Let us start by summarizing the basic equations of homogenization in application to the heat conduction problem. The scale transition between two levels (micro to macro) draws on splitting the local temperature field into macroscopic and fluctuation parts, respectively

$$t(\boldsymbol{x}) = t(\boldsymbol{x}^0) + T_{,i}(x_i - x_i^0) + t^*(\boldsymbol{x}), \tag{1}$$

where $T_{,i}$ are components of the macroscopically uniform temperature gradient vector and $t^*(\boldsymbol{x})$ is the fluctuation of the local temperature field (in this section the standard tensorial notation is used). Finally, $t(\boldsymbol{x}^0)$ is the temperature at the reference point $\boldsymbol{x}^0$. This formula immediately follows from the relation between the temperature gradients of individual fields

$$t_{,i}(\boldsymbol{x}) = T_{,i} + t^*_{,i}(\boldsymbol{x}). \tag{2}$$

The micro-temperature gradient averaged over the volume $|\Omega|$ of the representative volume element (RVE) with the boundary Γ,

$$\langle t_{,i} \rangle = \frac{1}{|\Omega|} \int_\Omega t_{,i}(\boldsymbol{x}) \, \mathrm{d}\Omega(\boldsymbol{x}) = T_{,i} + \frac{1}{|\Omega|} \int_\Omega t^*_{,i}(\boldsymbol{x}) \, \mathrm{d}\Omega(\boldsymbol{x}), \tag{3}$$

yields a scale transition relation, see e.g. (Oezdemir et al., 2006),

$$\langle t^*_{,i} \rangle = \frac{1}{|\Omega|} \int_\Omega t^*_{,i}(\boldsymbol{x}) \, \mathrm{d}\Omega(\boldsymbol{x}) = \frac{1}{|\Omega|} \int_\Gamma t^*(\boldsymbol{x}) \nu_i(\boldsymbol{x}) \, \mathrm{d}\Gamma(\boldsymbol{x}) = 0. \tag{4}$$

The boundary integral disappears providing either the fluctuating part of the temperature field equals zero (in the case of fully prescribed temperature and/or normal heat flux boundary conditions) or the periodic boundary conditions, i.e. the same values of t^* on opposite sides of a rectangular periodic unit cell (PUC) are enforced on Γ.

When discussing the micro to macro scale transition it is worth mentioning an analogy between the basic quantities related to the heat conduction problems (i.e. the negative values of temperature gradients $(-t_{,i})$ or $(-T_{,i})$ and fluxes q_i or Q_i as their conjugate measures) and the corresponding quantities applied to mechanical problems (strains ε_{ij} or E_{ij} and the conjugate stress measures σ_{ij} or Σ_{ij}). While homogenization of mechanical problems benefits from the Hill lemma

$$\dot{W} = \langle \dot{\varepsilon}_{ij} \sigma_{ij} \rangle = \dot{E}_{ij} \Sigma_{ij} \geq 0, \tag{5}$$

where $\dot{(\,)}$ represents the derivative with respect to time, the Fourier inequality

$$\dot{S}t = (-t_{,i}) q_i \geq 0, \tag{6}$$

is called to arrive at the counterpart of Eq. 5 as

$$\langle(-t_{,i})q_i\rangle = -T_{,i}Q_i \geq 0, \tag{7}$$

which is applicable in the case of homogenization of the heat conduction problems.

Following the transformation of the volume integral in Eq. 4 to its boundary equivalent it is useful to convert the left-hand side of Eq. 7 in a similar way

$$\begin{aligned}\langle t_{,i}q_i\rangle &= \frac{1}{|\Omega|}\int_\Omega t_{,i}(\boldsymbol{x})q_i(\boldsymbol{x})\,\mathrm{d}\Omega(\boldsymbol{x}) = \frac{1}{|\Omega|}\int_\Gamma t(\boldsymbol{x})q_i(\boldsymbol{x})\nu_i(\boldsymbol{x})\,\mathrm{d}\Gamma(\boldsymbol{x}) = \\ &= \frac{1}{|\Omega|}\int_\Gamma t(\boldsymbol{x})q_\nu(\boldsymbol{x})\,\mathrm{d}\Gamma(\boldsymbol{x}).\end{aligned} \tag{8}$$

The term

$$-\frac{1}{\Omega}\int_\Omega t(\boldsymbol{x})q_{i,i}(\boldsymbol{x})\,\mathrm{d}\Omega(\boldsymbol{x}), \tag{9}$$

has been omitted in Eq. 8 because of the balance of heat (i.e. $q_{i,i} = 0$ under steady state conditions and the absence of internal heat sources).

The same boundary conditions, which satisfy Eq. 4, lead to the equivalence of the volume averaged microscopic heat flux q_i and the macroscopic heat flux Q_i. To prove this, the well-known identity [1]

$$\int_\Omega q_i(\boldsymbol{x})\,\mathrm{d}\Omega(\boldsymbol{x}) = \int_\Gamma x_i q_\nu(\boldsymbol{x})\,\mathrm{d}\Gamma(\boldsymbol{x}), \tag{10}$$

is utilized. The following three situations can be distinguished:

- In the case of fully prescribed temperature boundary conditions, the subsequent combination of Eqs. 1, 8 and 10, in conjunction with the balance condition

$$\int_\Gamma q_\nu(\boldsymbol{x})\,\mathrm{d}\Gamma(\boldsymbol{x}) = 0, \tag{11}$$

  yields

$$\begin{aligned}\langle t_{,i}q_i\rangle &= \frac{t(\boldsymbol{x}^0)}{|\Omega|}\int_\Gamma q_\nu(\boldsymbol{x})\,\mathrm{d}\Gamma(\boldsymbol{x}) + \frac{T_{,i}}{|\Omega|}\int_\Gamma (x_i - x_i^0)q_\nu(\boldsymbol{x})\,\mathrm{d}\Gamma(\boldsymbol{x}) = \\ &= \frac{T_{,i}}{|\Omega|}\int_\Omega q_i(\boldsymbol{x})\,\mathrm{d}\Omega(\boldsymbol{x}) = T_{,i}Q_i.\end{aligned} \tag{12}$$

  This identity implies

$$Q_i = \frac{1}{|\Omega|}\int_\Omega q_i(\boldsymbol{x})\,\mathrm{d}\Omega(\boldsymbol{x}). \tag{13}$$

- A similar situation is met if normal heat flux boundary conditions are prescribed. Substituting the prescribed macroscopic flux Q_i into Eq. 12 for q_i immediately proves the validity of Eq. 13.

- The periodic temperature boundary conditions are typical of rectangular PUCs. From the transition relation 4, the fluctuation temperature t^* must be the same on the opposite boundaries of PUC. As the anti-periodic normal heat flux applies to the periodic boundary conditions, Eq. 12 yields, after certain modifications, the expected result 13.

[1] $\int_\Gamma x_i q_\nu(\boldsymbol{x})\,\mathrm{d}\Gamma(\boldsymbol{x}) = \int_\Gamma x_i q_j(\boldsymbol{x})\nu_j(\boldsymbol{x})\,\mathrm{d}\Gamma(\boldsymbol{x}) = \int_\Omega (x_i q_i(\boldsymbol{x}))_{,j}\,\mathrm{d}\Omega(\boldsymbol{x}) = \int_\Omega (\delta_{ij}q_j(\boldsymbol{x}) + x_i \underbrace{q_j(\boldsymbol{x})_{,j}}_{0})\,\mathrm{d}\Omega(\boldsymbol{x}) = \int_\Omega q_i(\boldsymbol{x})\,\mathrm{d}\Omega(\boldsymbol{x})$

3 Macroscopic conductivity and resistivity matrices

Before proceeding with the analysis of a complex coupled nonlinear heat and moisture conduction problem we review the basic steps for the evaluation of macroscopic conductivity and resistivity matrices through the solution of a simple steady state heat conduction problem. This allows us to examine the influence of various boundary conditions discussed in the previous section on the predicted homogenized properties and further exploit these results in the next section when solving the coupled problem.

3.1 Governing equations

Macroscopic conductivity and resistivity matrices may be derived by analogy to homogenized stiffness and compliance matrices which apply to mechanical FE analyses. Recall that the starting point for the latter case is the discretized form of the strain and stress vectors, respectively (henceforth the previously used tensorial notation is substituted by the matrix notation)

$$\boldsymbol{\varepsilon} = \boldsymbol{E} + \mathbf{B}_u \boldsymbol{r}_u^*, \quad \boldsymbol{\sigma} = \mathbf{L}\boldsymbol{\varepsilon}, \tag{14}$$

where $\boldsymbol{r}_u^*$ is the vector of the nodal values of the fluctuation displacement field, $\mathbf{B}_u$ stores derivatives of the displacement shape functions and $\mathbf{L}$ is the microscopic material stiffness matrix.

Let $\boldsymbol{E}$ be the prescribed macroscopic strain vector. The equality of mechanical powers at the microscopic and macroscopic levels, Eq. 5, then gives

$$\langle \mathbf{B}_u^{\mathsf{T}} \mathbf{L} \rangle \boldsymbol{E} + \langle \mathbf{B}_u^{\mathsf{T}} \mathbf{L} \mathbf{B}_u \rangle \boldsymbol{r}_u^* = \mathbf{0}. \tag{15}$$

Eliminating $\boldsymbol{r}_u^*$ yields, after simple manipulations, the macroscopic relation for the stress vector

$$\boldsymbol{\Sigma} = \langle \boldsymbol{\sigma} \rangle = \langle \mathbf{L}(\boldsymbol{E} + \mathbf{B}_u \boldsymbol{r}_u^*) \rangle = \mathbf{L}^{hom} \boldsymbol{E}, \tag{16}$$

where

$$\mathbf{L}^{hom} = \langle \mathbf{L} \rangle - \langle \mathbf{L}\mathbf{B}_u \rangle \langle \mathbf{B}_u^{\mathsf{T}} \mathbf{L} \mathbf{B}_u \rangle^{-1} \langle \mathbf{L}\mathbf{B}_u \rangle^{\mathsf{T}}, \tag{17}$$

is the homogenized (macroscopic) material stiffness matrix.

If the macroscopic stress $\boldsymbol{\Sigma}$ is prescribed a similar procedure applies and arrives at a set of the following equations for unknown $\boldsymbol{E}$ and $\boldsymbol{r}_u^*$

$$\begin{aligned} \langle \mathbf{L} \rangle \boldsymbol{E} + \langle \mathbf{L}\mathbf{B}_u \rangle \boldsymbol{r}_u^* &= \boldsymbol{\Sigma}, \\ \langle \mathbf{L}\mathbf{B}_u \rangle^{\mathsf{T}} \boldsymbol{E} + \langle \mathbf{B}_u^{\mathsf{T}} \mathbf{L} \mathbf{B}_u \rangle \boldsymbol{r}_u^* &= \mathbf{0}. \end{aligned} \tag{18}$$

Again, eliminating $\boldsymbol{r}_u^*$ readily provides the macroscopic relation

$$\boldsymbol{E} = \mathbf{C}^{hom} \boldsymbol{\Sigma}, \tag{19}$$

where $\mathbf{C}^{hom} = (\mathbf{L}^{hom})^{-1}$ is the macroscopic material compliance matrix.

In view of the analogy mentioned at the beginning of this section we first discretize the temperature gradient and the heat flux vector, respectively, as

$$\boldsymbol{\nabla} t = \boldsymbol{\nabla} T + \mathbf{B}_t \boldsymbol{r}_t^*, \quad \boldsymbol{q} = -\boldsymbol{\chi} \boldsymbol{\nabla} t, \tag{20}$$

where $\boldsymbol{\nabla}^{\mathsf{T}} = \left[\frac{\partial}{\partial x}, \frac{\partial}{\partial y}, \frac{\partial}{\partial z} \right]$, $\boldsymbol{r}_t^*$ is a vector of the nodal values of the fluctuation temperature field, $\boldsymbol{\chi}$ is the microscopic conductivity matrix and entries of the matrix $\mathbf{B}_t$ represent the derivatives of the temperature shape functions.

Let $\boldsymbol{\nabla} T$ be the prescribed macroscopic temperature gradient. Then the equality given by Eq. 7 results in (compare with Eq. 15)

$$\langle \mathbf{B}_t^{\mathsf{T}} \boldsymbol{\chi} \rangle \boldsymbol{\nabla} T + \langle \mathbf{B}_t^{\mathsf{T}} \boldsymbol{\chi} \mathbf{B}_t \rangle \boldsymbol{r}_t^* = \mathbf{0}, \tag{21}$$

and, successively, in the macroscopic relation for the heat flux

$$\boldsymbol{Q} = \langle \boldsymbol{q} \rangle = -\langle \boldsymbol{\chi} (\boldsymbol{\nabla} T + \mathbf{B}_t \boldsymbol{r}_t^*) \rangle = -\boldsymbol{\chi}^{hom} \boldsymbol{\nabla} T, \tag{22}$$

where (compare with Eq. 17)

$$\boldsymbol{\chi}^{hom} = \langle \boldsymbol{\chi} \rangle - \langle \boldsymbol{\chi} \mathbf{B}_t \rangle \langle \mathbf{B}_t^{\mathsf{T}} \boldsymbol{\chi} \mathbf{B}_t \rangle^{-1} \langle \boldsymbol{\chi} \mathbf{B}_t \rangle^{\mathsf{T}}, \tag{23}$$

is the effective (macroscopic) conductivity matrix.

If the macroscopic flux, $\boldsymbol{Q}$, is prescribed, Eq. 7 first leads to

$$\begin{aligned} \langle \boldsymbol{\chi} \rangle \boldsymbol{\nabla} T + \langle \boldsymbol{\chi} \mathbf{B}_t \rangle \boldsymbol{r}_t^* &= -\boldsymbol{Q}, \\ \langle \boldsymbol{\chi} \mathbf{B}_t \rangle^{\mathsf{T}} \boldsymbol{\nabla} T + \langle \mathbf{B}_t^{\mathsf{T}} \boldsymbol{\chi} \mathbf{B}_t \rangle \boldsymbol{r}_t^* &= \mathbf{0}, \end{aligned} \tag{24}$$

and then, similarly as in the case of Eq. 19, to the macroscopic equation

$$\boldsymbol{\nabla} T = -\boldsymbol{\Psi}^{hom} \boldsymbol{Q}, \tag{25}$$

where $\boldsymbol{\Psi}^{hom} = (\boldsymbol{\chi}^{hom})^{-1}$ is the effective (macroscopic) resistivity matrix.

3.2 Periodic boundary conditions in commercial codes

Recall that the effective thermal conductivities have been derived based on the additive split of the temperature field in the form 1. Such a decomposition, although advantageous from the point of view of theoretical considerations, is, however, rather difficult to correctly introduce into most of the commercial codes available. Therefore, an alternative approach to impose the periodicity constraints as well as the overall (macroscopic) gradient $\boldsymbol{\nabla} T$ is on demand. To this end, consider a two-dimensional rectangular PUC with dimensions H and L (see Fig. 1).

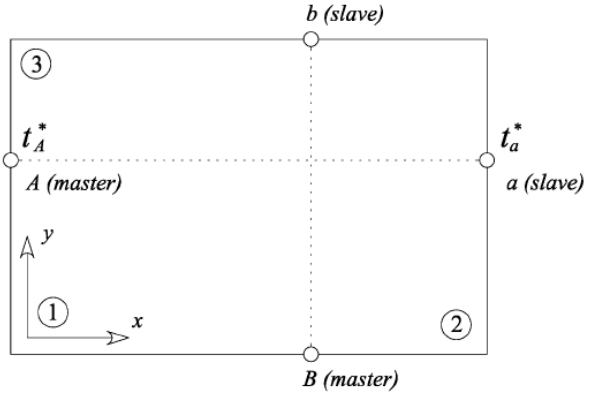

Figure 1: Conditions of periodicity

mortar	stone
2.0	0.9

Table 1: Phase conductivities $\chi[\mathrm{Wm}^{-1}\mathrm{K}^{-1}]$

Observe that for a pair of points (e.g. A - master and a - slave) located on the opposite sides of the PUC the following relations hold:

$$t_A = \left(\frac{\partial T}{\partial y}\right) y_A + t_A^* + t(\boldsymbol{x}^0), \quad t_a = \left(\frac{\partial T}{\partial x}\right) L + \left(\frac{\partial T}{\partial y}\right) y_a + t_a^* + t(\boldsymbol{x}^0). \tag{26}$$

Taking into account the fact that the fluctuating field t^* satisfies the periodicity condition

$$t_a^* = t_A^*, \tag{27}$$

and subtracting corresponding terms on the opposite edges, we finally obtain (compare with (Oezdemir et al., 2006))

$$\left(\frac{\partial T}{\partial x}\right) L = t_a - t_A = t_2 - t_1, \tag{28}$$

$$\left(\frac{\partial T}{\partial y}\right) H = t_b - t_B = t_3 - t_1. \tag{29}$$

These conditions can be introduced into most commercial software products using the multi-point constrain equations.

3.3 Influence of boundary conditions on effective conductivities

To capture the influence of the selected type of boundary conditions consider an RVE displayed in Fig. 2. Such a meso-structure does not represent a typical masonry bonding, as in this scheme both the stone blocks and bed joints are regularly and uniformly distributed. It is also worth noting that such an arrangement is not perfectly periodic due to the disturbance of periodicity along the boundary. This large RVE has been deliberately chosen to demonstrate certain edge effects, which may be taken into account when homogenization is carried out using commercial and/or academic computer codes. If the RVE was perfectly periodic (i.e. one half of the boundary mortar joint was added as sketched by the dashed line in Fig. 2), then, due to the infinite periodicity, any stone block along with the adjacent part of bed and head joints shaded in Fig. 2 would be sufficient for calculating the effective value of thermal conductivity.

In this simple case the cross-effects between the heat and moisture were omitted. The phase thermal conductivities are listed in Table 1. First, the effect of imperfect periodicity was studied by loading the large RVE in Fig. 2 by a uniform macroscopic temperature gradient $\nabla_x T = 1$ while setting $\nabla_y T = 0$. Fully prescribed boundary temperatures were considered so that $t^* = 0$. The fluctuating temperature field displayed in Fig. 3(a) was found from the solution of Eq. 21. Note that the imperfect periodicity of the RVE (the edge effect) manifests itself in slightly affecting the periodicity of the fluctuating field t^*. Fig. 3(b) shows similar results derived by discretizing only the PUC. Finally, the results plotted in Fig. 3(c) were generated again through the solution of the unit cell problem but assuming periodic boundary conditions.

The corresponding effective thermal conductivities were obtained directly from Eq. 23. Individual values are stored in Table 2 clearly suggesting, at least in this particular example, the invariance of the predicted effective thermal conductivities on the choice of specific boundary conditions. This appealing result will be further exploited in the next section.

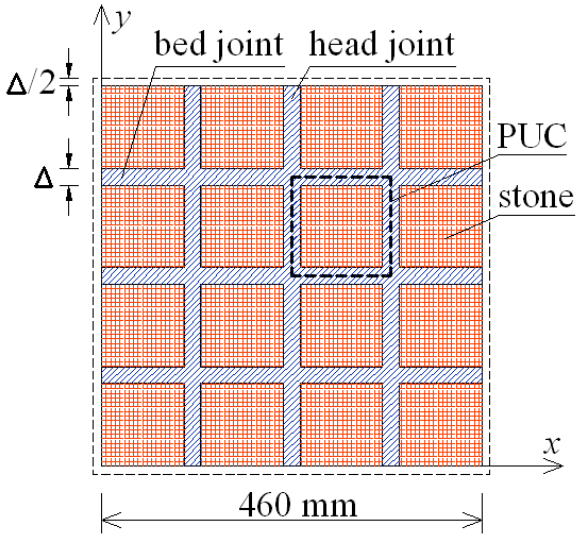

Figure 2: Meso-structure consisting of stone blocks and mortar joints

No periodicity	PUC $t^* = 0$ on Γ_t	PUC t^*-periodic
1.113	1.169	1.167

Table 2: Effective conductivities $\chi_x^{hom}[\mathrm{Wm^{-1}K^{-1}}]$

4 Effect of moisture on thermal conductivity

So far we restrained our attention to heat conduction problems under steady state conditions. To this end, the balance equation, $q_{i,i} = 0$, Fourier's law and the equivalence of heat powers on micro- and macro-scales, Eq. 7, were sufficient to derive both effective conductivity and resistivity matrices. When analyzing large structural systems, such as historical stone bridges, cathedrals and similar historical structures, the effect of moisture must be taken into consideration and, therefore, the solution of the coupled heat and moisture transfer is desirable.

4.1 Basic equations for coupled mass and energy transfer

In this paragraph we briefly outline the basic equations from which the computational approaches come from. Considering a variety of models discussed in the introductory part of this paper we focus on the model by Lewis and Schrefler, see Lewis and Schrefler (1999). This model, which describes the coupled moisture and heat transfer in deforming porous media, was for practical applications implemented, along with Künzel and Kiessel's model Künzel and Kiessl (1997), into the SIFEL (SImple Finite ELements Kruis et al. (2003)) computer code developed at our department. In general, the complete set of equations comprises the linear balance (equilibrium) equation formulated for a multiphase body, the energy balance equation and the continuity equations for liquid water and gas. In this paper, being concerned with a coupled heat and moisture transfer only, the list of equations is reduced by assuming the rigidity of the solid phase.

When dealing with the phase exchange, it is more convenient to express the energy balance by means of the specific enthalpy. If some insignificant terms are neglected and providing the local equilibrium state holds ($t^\alpha = t, \alpha = w, g$; $w \equiv$ water, $g \equiv$ gas), we arrive at the balance

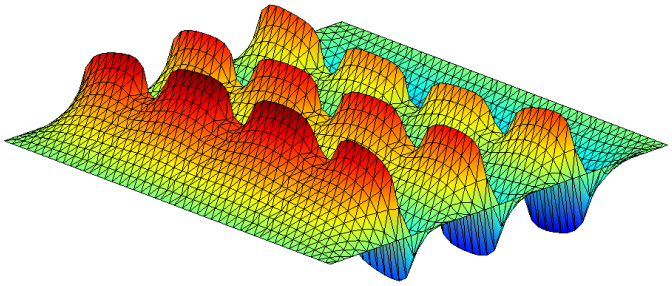

(a)

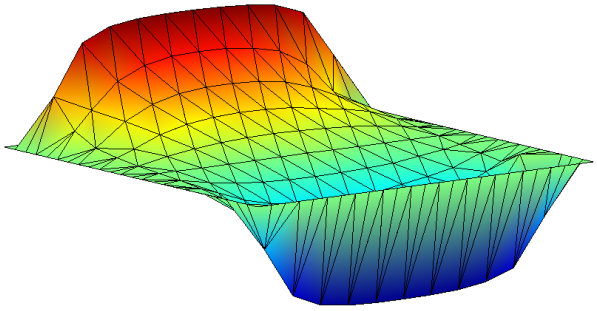

(b)

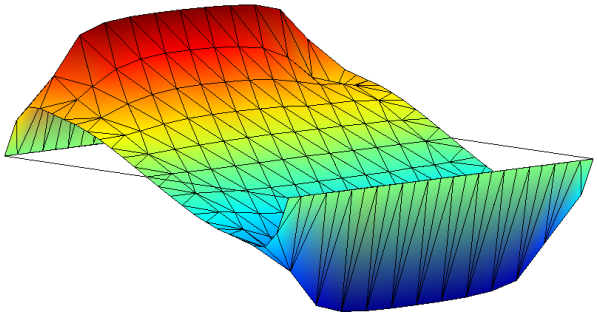

(c)

Figure 3: Fluctuating temperature field: (a) large RVE and $t^* = 0$ (b) PUC and $t^* = 0$ (c) PUC and t^*-periodic

equation in this form

$$(\rho C_p)\dot{t} + (\rho_w C_p^w \boldsymbol{v}^w + \rho_g C_p^g \boldsymbol{v}^g)^{\mathsf{T}} \boldsymbol{\nabla} t + \boldsymbol{\nabla}^{\mathsf{T}}(-\boldsymbol{\chi}\boldsymbol{\nabla} t) = -\dot{m}\Delta H_{vap}, \tag{30}$$

where ΔH_{vap} is the latent heat of evaporation and $\dot{m}$ is the mass rate of evaporation. In Eq. 30, the coefficients C_p^α represent the specific heat capacity of individual phases, $\boldsymbol{v}^\alpha$ are the corresponding phase velocities and, finally, the effective heat capacity is expressed as

$$\rho C_p = \rho_s C_p^s + \rho_w C_p^w + \rho_g C_p^g. \tag{31}$$

When coupling between the heat and moisture is considered the energy balance equation 30 must be accompanied by the continuity equations for liquid and gas phases derived from the corresponding mass balance equations. The continuity equation for the liquid phase, see also (Lewis and Schrefler, 1999; Krejčí et al., 2001), is provided by

$$\begin{aligned} &\frac{nS_w}{K_w}\dot{p}^w - S_w\left[(1-n)\,\beta_s + n\beta_w\right]\dot{t} + n\dot{S}_w + \\ &+\boldsymbol{\nabla}^{\mathsf{T}}\left[\frac{\boldsymbol{k}k^{rw}}{\mu^w}\left(-\boldsymbol{\nabla}p^w + \rho^w\boldsymbol{g}\right)\right] = -\frac{\dot{m}}{\rho^w}, \end{aligned} \tag{32}$$

where p^w is the pressure of the liquid water. The continuity equation for gas is expressed in a similar manner. The final result reads

$$\begin{aligned} &-n\dot{S}_w - S_g(1-n)\beta_s\dot{t} + \frac{nS_g}{\rho^g}\left[\frac{p^g M_g}{\hat{\theta}R}\right]^{\cdot} + \\ &+\boldsymbol{\nabla}^{\mathsf{T}}\left[\frac{\boldsymbol{k}k^{rg}}{\mu^g}\left(-\boldsymbol{\nabla}p^g + \rho^g\boldsymbol{g}\right)\right] = \frac{\dot{m}}{\rho^g}, \end{aligned} \tag{33}$$

where p^g is the pressure of gas. In Eqs. 32 and 33 K_w is the bulk modulus of water, β_s and β_w are the relevant coefficients of thermal expansion, (nS_w) and (nS_g) are the volume fractions of the liquid water and gas (moist air), n is the porosity, ρ^w, ρ^g stand for the intrinsic phase densities, $\hat{\Theta}$ is the absolute temperature, R is the universal gas constant and M_g is the molar mass of moist air. Saturation S_w and $S_g = 1 - S_w$ can be eliminated by means of the retention formula $p^c = p^c(S_w, t)$, where $p^c = p^g - p^w$ is the capillary pressure (suction). The last terms on the left hand side of both continuity equations represent the mass fluxes of water and gas, respectively, expressed by particular forms of Darcy's law (Lewis and Schrefler, 1999; Krejčí et al., 2001); $\boldsymbol{k}$ is the permeability matrix of a fully saturated medium, $k^{r\alpha}$ is the relative permeability and μ^α is the dynamic viscosity of a given phase $\alpha = w, g$.

As evident from the structure of continuity equations 32 and 33 we consider a porous system with incompressible grains and neglect the volumetric deformation of the porous skeleton ($\mathrm{div}\boldsymbol{v}_s = 0$) as well as the gradient of the water density. The fundamental unknowns in the theory of the coupled moisture and heat transfer are then represented by

- the temperature t
- the pressures in the liquid and gas phase, respectively, p^w, p^g.

The three unknown functions, defined in a domain Ω with a boundary Γ, can be solved from three basic equations

- one energy balance equation 30

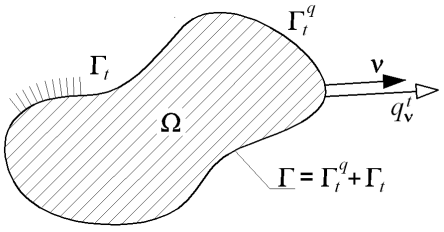

Figure 4: A 2D region (a PUC in our case) with imposed heat flux q_ν

- two continuity equations 32 and 33.

To arrive at computational simulations the system of equations 30, 32 and 33 must be converted to a weak formulation. To this end, the weighted residual statement is used along with Green's theorem applied to the terms containing the divergence operator. After these manipulations, the energy balance equation takes this form

$$\int_\Omega \left\{ w_t \left[(\rho C_p)\dot{t} + (\rho_w C_p^w \boldsymbol{v}^w + \rho_g C_p^g \boldsymbol{v}^g)^\mathsf{T} \boldsymbol{\nabla} t + \dot{m} \Delta H_{vap} \right] + \right. \\ \left. + (\boldsymbol{\nabla}^\mathsf{T} w_t)(\boldsymbol{\chi} \boldsymbol{\nabla} t) \right\} \, \mathrm{d}\Omega + \int_{\Gamma_t^q} w_t q_\nu^t \, \mathrm{d}\Gamma = 0, \tag{34}$$

where w_t is the weighting function such that $w_t = 0$ on Γ_t and q_ν^t is the heat flux perpendicular to the boundary Γ_t^q, see Fig. 4. The weak formulation for the continuity equations can be obtained similarly. The respective formula to the continuity equation for liquid water is provided by

$$\int_\Omega \left\{ w_p \left[\frac{n S_w}{K_w} \dot{p}^w - S_w \left[(1-n)\, \beta_s + n \beta_w \right] \dot{t} + n \dot{S}_w + \frac{\dot{m}}{\rho^w} \right] + \right. \\ \left. + (\boldsymbol{\nabla}^\mathsf{T} w_p) \frac{\boldsymbol{k} k^{rw}}{\mu^w} \left(\boldsymbol{\nabla} p^w - \rho^w \boldsymbol{g} \right) \right\} \, \mathrm{d}\Omega + \int_{\Gamma_w^q} w_p \frac{q_\nu^w}{\rho^w} \, \mathrm{d}\Gamma = 0, \tag{35}$$

where q_ν^w is the boundary liquid water flux and w_p is the corresponding weighting function. Finally, the integral formula to the continuity equation for gas reads

$$\int_\Omega \left\{ w_p \left[-n \dot{S}_w - S_g (1-n) \beta_s \dot{t} + \frac{n S_g}{\rho^g} \left[\frac{p^g M_g}{\hat{\theta} R} \right]^{\cdot} - \frac{\dot{m}}{\rho^g} \right] + \right. \\ \left. + (\boldsymbol{\nabla}^\mathsf{T} w_p) \frac{\boldsymbol{k} k^{rg}}{\mu^g} \left(\boldsymbol{\nabla} p^g - \rho^g \boldsymbol{g} \right) \right\} \, \mathrm{d}\Omega + \int_{\Gamma_g^q} w_p \frac{q_\nu^g}{\rho^g} \, \mathrm{d}\Gamma = 0. \tag{36}$$

Again, considering the retention formula, $p^c = p^c(S_w, t)$, allows us to express the derivative of the degree of saturation as

$$\dot{S}_w = \frac{\partial S_w}{\partial p^c} (\dot{p}^g - \dot{p}^w) + \frac{\partial S_w}{\partial t} \dot{t}. \tag{37}$$

4.2 Effective conductivities as a function of relative humidity and initial temperature

Owing to the results derived in Section 3.3 (the fully prescribed temperature boundary conditions provide sufficiently accurate results so there is no need to deal with the periodic boundary conditions) it appears advantageous to exploit one of the available commercial or academic computer codes when solving the system of equations 34 through 36.

There exist a number of such codes that allow for the description of non-linear and non-stationary material behavior as well as cross - effects when studying the moisture and heat transfer in heterogeneous infrastructures. As two representatives of various numerical techniques we recall the FEM based program SIFEL (Kruis et al., 2003) and program DELPHIN (Grunewald, 1997, 2000) developed on the basis of the finite control volume method (FCVM).

Because of a limited extent of this paper only the results of a case study are presented. Keeping in mind that the fully prescribed temperature or fully prescribed fluxes are corresponding dual boundary conditions, the RVE shown in Fig. 2 is again used and subjected in this case to a unidirectional heat flux q_x while isolating the horizontal boundaries $q_y = 0$. The total temperature field $t = T + t^*$, which corresponds to $q_x = 100\mathrm{Wm}^{-2}$, appears in Fig. 5. In this case the room initial temperature $t_{in} = 25°\mathrm{C}$ and relative humidity $\varphi = 60\%$ were considered. The results obtained hereafter were calculated with the help of the DELPHIN computer code. Nevertheless, almost the same result was obtained when employing the SIFEL program.

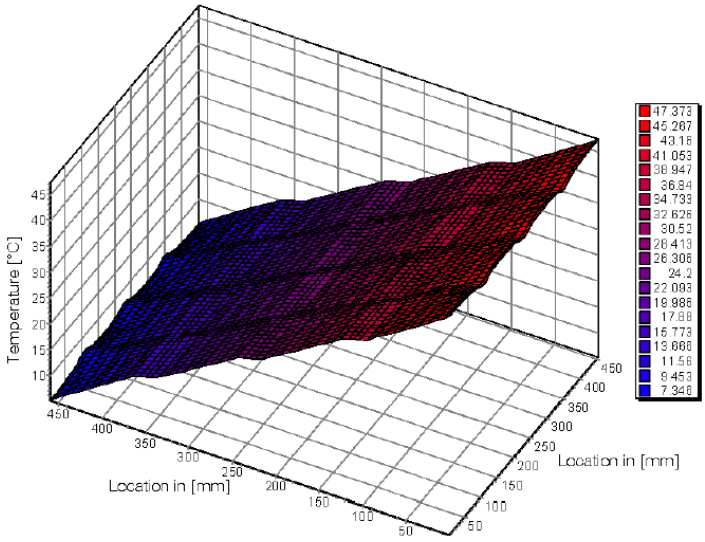

Figure 5: Total temperature field produced by flux $q_x = 100\mathrm{Wm}^{-2}$

As evident from Fig.6, the volume moisture field $w\,(\mathrm{m}^3/\mathrm{m}^3)$ considerably varies throughout the RVE thus affecting the macroscopic thermal conductivity slightly depending on the size of the RVE. Here the thermal conductivity was derived from Eq. 22 by dividing the prescribed heat flux by the temperature gradient found from Eq. 3 when reaching the steady state conditions.

Several interesting results have been derived within the scope of our numerical experiments. The graph in Fig. 7(a) displays the dependence of the macroscopic heat conductivity χ^{hom} on the average relative humidity φ. Individual values of χ^{hom} follow again from Eq. 22.

It should be pointed out that the nearly linear dependence between these two variables at a sub-hygroscopic region (up to about 95% - 98%) becomes highly non-linear once the hygroscopic moisture is attained and approaches the capillary and even maximum (vacuum) saturation.

Fig. 7(b) displays the relation between the macroscopic thermal conductivity and the initial temperature for different levels of the relative humidity φ.

Finally, note a very important finding of considerable practical significance that follows

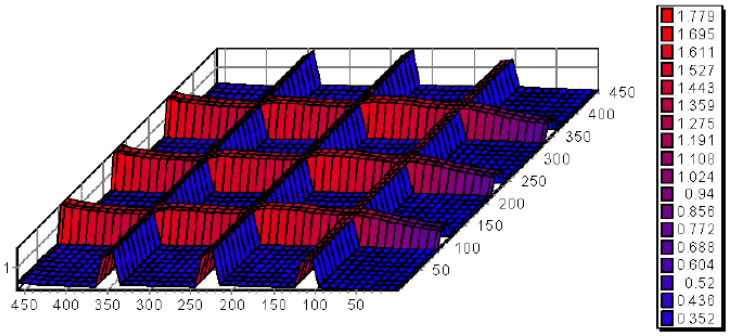

Figure 6: Distribution of volume moisture $w\,(\mathrm{m}^3/\mathrm{m}^3)$; $q_x = 100\mathrm{Wm}^{-2}$, $t_{in} = 25°\mathrm{C}$

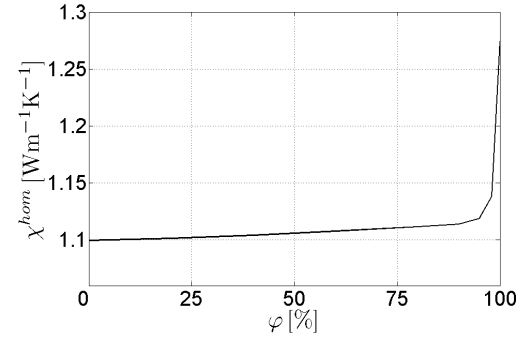

(a)

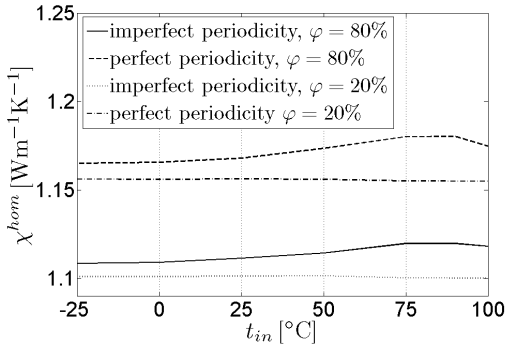

(b)

Figure 7: Evolution of χ^{hom} as a function of: (a) φ at $t_{in} = 25°\mathrm{C}$, (b) t_{in} at $\varphi = 20\%$ and $\varphi = 80\%$

from our numerical tests - the coefficient of the macroscopic thermal conductivity χ^{hom} is almost insensitive to the changes in the macroscopic temperature gradient $\boldsymbol{\nabla} t$, which simplifies the micro (meso)-macro approach.

5 Further developments - heat and moisture transfer across interfaces

Another important matter, which has not yet been satisfactorily settled, is the heat and moisture transfer across interfaces. To date the following three ways have mostly been considered when solving this problem (in what follows the symbol $[\![\cdot]\!]$ is used to denote a jump of a quantity across an interface (Černý and Rovnaníková, 2002)):

1. A continuity of relative humidity across the interface $[\![\varphi]\!] = 0$ is enforced, see (Krischer, 1963). However, this condition is valid in the hygroscopic range only, where a sorption isotherm can be employed.

2. To start from the classical definition of a hydraulic contact, see (Černý and Rovnaníková, 2002), we assume $[\![p^c]\!] = 0$. At the interface between two distinct materials, this condition leads to a moisture jump across the interface, which can be derived from the function $p^c = p^c(w)$.

3. On the other hand a non-ideal hydraulic contact on the interface manifests itself by the different pore size distributions of the adjacent porous materials (Fig. 8). Such an "imperfect" contact entails a jump of capillary pressure along the interface (Bear and Bachmat, 1990)

$$[\![p^c]\!] = -\frac{j_{if}}{k_{if}}, \tag{38}$$

where $j_{if} = j_+ = j_-$ is the moisture flux across the interface in the normal direction and k_{if} is a macroscopic parameter known as the interface permeability.

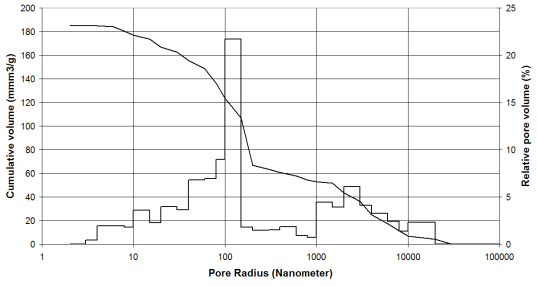

(a)

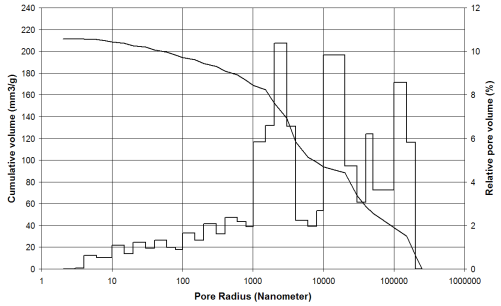

(b)

Figure 8: Pore size distributions of two contiguous materials: (a) arenaceous marl, (b) mortar

Fig. 8 shows the pore size distribution for two different materials. It is evident that the third model is the most pertinent to the description of the heat and mass transfer across the interface

in masonry structures. It is plain enough to expect that the jump in capillary pressure across an interface results in a corresponding jump in the temperature as schematically shown in Fig. 9, so that

$$[\![t]\!] = -\frac{j_{Qif}}{\alpha_{if}}, \tag{39}$$

where $j_{Qif} = j_{Q+} = j_{Q-}$ is the heat flux across the interface in the normal direction and α_{if} is again a material parameter known as the internal transfer coefficient.

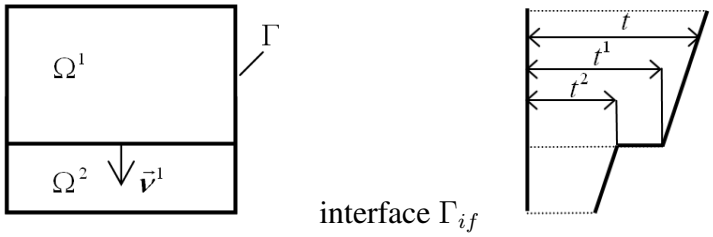

Figure 9: A sample composed of two materials (s, m)

The meaning of the two material parameters k_{if} and α_{if} becomes evident as soon as we assign the weighted residual statements to the local balance equations describing the heat and moisture transfer in masonry, Eqs. 34 - 36.

For illustration consider the internal transfer coefficient. Eq. 34 is now written for both adjacent materials, mortar and stone. Applying the Gauss theorem to the convective terms, assuming that $w_t = 0$ on Γ_t (fully prescribed external temperature boundary conditions), and finally adding the convective terms of both sub-domains, while noticing $\boldsymbol{\nu}^2 = -\boldsymbol{\nu}^1$, yields

$$\begin{aligned} \cdots + \int_{\Gamma_{if}} \left[\!\left[(\rho_w C_p^w \boldsymbol{v}^w + \rho_g C_p^g \boldsymbol{v}^g) t w_t\right]\!\right]^{\mathsf{T}} \boldsymbol{\nu}^1 \mathrm{d}\Gamma_{if} \cdots = \\ = \cdots \int_{\Gamma_{if}} j_{Qif} \, [\![w_t]\!] \, \mathrm{d}\Gamma_{if} \cdots = 0. \end{aligned} \tag{40}$$

From the requirement of a continuous transition of fluxes we obtain

$$\begin{aligned} j_{Qif} &= (\rho_w^1 C_p^{w1} \boldsymbol{v}^{w1} + \rho_g^1 C_p^{g1} \boldsymbol{v}^{g1})^{\mathsf{T}} t^1 \boldsymbol{\nu}^1 = \\ &= (\rho_w^2 C_p^{w2} \boldsymbol{v}^{w2} + \rho_g^2 C_p^{g2} \boldsymbol{v}^{g2})^{\mathsf{T}} t^2 \boldsymbol{\nu}^1. \end{aligned} \tag{41}$$

The conversion of the local moisture balance equations for the liquid water and gas (a mixture of water vapor and dry air) will be treated in a similar way utilizing the well known capillary pressure equation

$$p^c = p^w - p^g < 0, (\text{suction}).$$

where p^g and p^w is the pressure of the gaseous phase and the liquid water, respectively. This is a subject of our further work.

6 Conclusions

Homogenization techniques applied to a meso-scale provide the values of effective transport parameters, such as the coefficient of thermal conductivity (and/or moisture permeability), and allow for their dependence on both macroscopic temperature and moisture fields. As efficient

tools, the DELPHIN and SIFEL computer codes can be effectively used when analyzing transport processes within a certain PUC to get distributions of these fields on a meso-scale, while taking into account the cross-effects in transport phenomena. With reference to thermal conductivity the following conclusions can be pointed out:

- At low levels of moisture the coefficient of thermal conductivity varies almost linearly with the relative humidity φ. This relation becomes strongly non-linear as soon as the hygroscopic moisture ($\varphi \approx 95\%$) is attained.
- The macroscopic volume moisture ($\mathrm{m}^3/\mathrm{m}^3$) extensively varies throughout the RVE thus affecting the value of macroscopic thermal conductivity.
- There exists a certain dependence of the macroscopic thermal conductivity on the initial temperature t_{in}. But it is distinctive just at higher temperatures, say above $30°\mathrm{C}$.
- A very important finding is that the macroscopic conductivity is nearly insensitive to the macroscopic temperature gradient, even in the non-linear range, which simplifies the meso-macro approach.

7 Acknowledgment

This outcome has been achieved with the financial support of the Ministry of Education, Youth and Sports, project No. 1M0579, within activities of the CIDEAS research centre. In this undertaking, theoretical results gained in the project GAČR 103/04/1321 and 103/08/1531 were partially exploited.

8 References

Auriault, J. (1983). Effective macroscopic description for heat conduction in periodic composites. *International Journal of Heat Mass Transfer*, 26:861–869.

Bear, J. and Bachmat, Y. (1990). *Introduction to modeling of transport phenomena in porous media*. Kluwer Academic Publishers, Dordrecht.

Biot, M. (1941). General theory of three-dimensional consolidation. *J. Appl. Phys.*, 12:155–164.

Boutin, C. (1995). Microstructural influence on heat conduction. *International Journal of Heat Mass Transfer*, 38:3181–3195.

De Boer, R. (1996). Highlights in the historical development of the porous media theory: toward a consistent macroscopic theory. *Applied Mechanical Review*, 49:201–262. Submitted.

Grunewald, J. (1997). *Diffusiver und konvektiver Stoff- und Energietransport in kapillarporsen Baustoffen*. PhD thesis, TU Dresden.

Grunewald, J. (2000). *DELPHIN 4.1 Documentation, Theoretical fundamentals*. Dresden:, TU Dresden.

Hassanizadech, M. and Gray, W. (1979a). General conservation equations for multiphase systems: 1, averaging procedure. *Adv. Water Resources*, 2:131–144.

Hassanizadech, M. and Gray, W. (1979b). General conservation equations for multiphase systems: 2, mass, momenta, energy and entropy equations. *Adv. Water Resources*, 2:191–203.

Kaminski, M. (2003). Homogenization of transient heat transfer problems for some composite materials. *International Journal of Engineering Science*, 41:1–29.

Krejčí, T., Nový, T., Sehnoutek, L., and Šejnoha, J. (2001). *Structure - subsoil interaction in view of transport processes in porous media*, volume 5 of *CTU Reports*. CTU in Prague. 81 pp.

Krischer, O. (1963). *Die wissentschaftliche Grundlagen der Trocknugstechnik*. Berlin:Springer Verlag, 2. auflage edition.

Kruis, J., Krejčí, T., and Bittnar, Z. (2003). Numerical solution of coupled problems. In Topping, B., editor, *Proceedings of The Ninth International Conference on Civil and Structural Engineering Computing*. Civil-Comp Press. on CD ROM.

Künzel, H. and Kiessl, K. (1997). Calculation of heat and moisture transfer in exposed building components. *International Journal of Heat Mass Transfer*, 40:159–167.

Lewis, R. W. and Schrefler, B. A. (1999). *The Finite Element Method in the Static and Dynamic Deformation and Consolidation of Porous Media*. John Wiley&Sons, Chichester, England, 2nd edition.

Novák, J., Zeman, J., Šejnoha, M., and Šejnoha, J. (2007). Pragmatic multi-scale and multi-physics analysis of charles bridge in prague. *Engineering Structures*, 0:0–0. Submitted.

Oezdemir, I., Brekelmans, W. A. M., and Geers, M. G. D. (2006). Computational homogenization for heat conduction in heterogeneous solids. *International journal for numerical methods in engineering*, 0:0–0. Article in press, http://dx.doi.org/10.1002/nme.2068.

Philip, J. and de Vries, D. (1957). Moisture movement in porous materials under temperature gradients. *Transaction of the American Geophysical Union*, 38:222–232.

Sýkora, J., Vorel, J., Šejnoha, J., and Šejnoha, M. (2005). Effective material parameters for transport processes in historical masonry structures. In Topping, B. H. V., editor, *Proceedings of the Tenth International Conference on Civil, Structural and Environmental Engineering Computing*, Stirling, United Kingdom. Civil-Comp Press. paper 190.

Tomková, B., Šejnoha, M., Novák, J., and Zeman, J. (2007). Evaluation of effective thermal conductivities of porous textile composites. *Composites - Part B:*, 0:0–0. Submitted.

Černý, R. and Rovnaníková, P. (2002). *Transport Processes in Concrete*. London: Spon Press.

Šejnoha, J., Zeman, J., Novák, J., and Janda, Z. (2005). Non-linear three-dimensional analysis of the charles bridge exposed to temperature impact. In Topping, B. H. V., editor, *Proceedings of the Tenth International Conference on Civil, Structural and Environmental Engineering Computing*, Stirling, United Kingdom. Civil-Comp Press. paper 187.